Lithos 323 (2018) 125–136

Contents lists available at ScienceDirect

Lithos

journal homepage: www.elsevier.com/locate/lithos

Chlorine-rich amphibole in deep layered gabbros as evidence for brine/rock interaction in the lower oceanic crust: A case study from the Wadi Wariyah, Samail Ophiolite, Sultanate of Oman

Adriana Currin [a,*], Paul Eric Wolff [a], Juergen Koepke [a], Renat R. Almeev [a], Chao Zhang [a], Barbara Zihlmann [b], Benoit Ildefonse [c], Damon A.H. Teagle [b]

[a] Leibniz Universität Hannover, Institut für Mineralogie, Callinstr. 3, Hannover D-30167, Germany
[b] School of Ocean and Earth Science, National Oceanography Centre Southampton, University of Southampton, Southampton SO14-3ZH, United Kingdom
[c] Géosciences Montpellier, CNRS, University of Montpellier, Université des Antilles, Montpellier, France

ARTICLE INFO

Article history:
Received 26 May 2018
11 September 2018
Accepted 12 September 2018
Available online 25 September 2018

Keywords:
Cl-bearing amphibole
High-temperature hydrothermal circulation
Lower oceanic crust
Samail Ophiolite
Phase separation
Brine-rock interactions

ABSTRACT

Hydrothermal veins and dykelets that cross-cut layered olivine gabbros deep in the plutonic section of the Samail Ophiolite, Sultanate of Oman, point towards the occurrence of hydrothermal circulation in the deep oceanic crust, and these features record interactions between rock and high temperature seawater-derived fluids or brines. Deep penetration of seawater-derived fluids down to 100 m above the Moho transition zone and the consequent interactions with the host rock lead to hydrothermal alteration from granulite facies grading down to greenschist facies conditions. Here we present a study of veins and dykelets formed by hydrothermal interaction cutting layered gabbro in the Wadi Wariyah, using petrographic, microanalytical, isotopic, and structural methods. We focus on amphiboles, which show a conspicuous compositional variation from high-Ti magnesiohastingsite and pargasite via magnesiohornblende and edenite, to Cl-rich ferropargasite and hastingsite (up to 1.5 a.p.f.u. Cl) and actinolite. These minerals record a wide range of formation conditions from magmatic to hydrothermal, and reveal a complex history of interactions between rock and hydrothermal fluid or brine in a lower oceanic crustal setting. Large variations in Cl content and cation configurations in amphibole suggest formation in equilibrium with fluids of different salinities at variable fluid/rock ratios. The presence of subsolidus amphibole extremely enriched in chlorine implies phase separation and brine/rock interactions. $^{87}Sr/^{86}Sr$ values of 0.7031 to 0.7039 and stable $\delta^{18}O$ isotopic compositions of 4.1 to 5.6‰ of the different amphibole types suggest a rock-dominated environment, i.e. with low fluid/rock ratios. However, the slight departure from mean Oman isotope values may indicate there was some influence of seawater in the aforementioned fluid-rock interactions. Our study provides new petrological data for the subsolidus evolution of gabbro-hosted amphibole-rich veins in the presence of a seawater-derived fluid.

1. Introduction

Fluid/rock interactions play an important role in mineral genesis and hydrothermal alteration at mid-ocean ridges, and are major contributors to heat and mass transfer control in the oceanic crust. Hydrothermal circulation occurs in the oceanic crust through the percolation of seawater into joints and fault zones in the seafloor (Manning and MacLeod, 1996; Manning et al., 2000). Several investigations argue that hydrothermal circulation is not restricted to the upper oceanic crust of fast-spreading mid-ocean ridges, but probably reaches beyond the sheeted dyke complex and down into the gabbro section (Fig. 1) (Gregory and Taylor, 1981; Harris et al., 2017; Zhang et al., 2014, 2017b). This is backed up by different types of studies, including field research on ophiolites (Gregory and Taylor, 1981; Bosch et al., 2004; Nicolas et al., 2003; Abily et al., 2011), analysis of drill cores obtained from the recent oceans (Alt and Bach, 2006; Coogan et al., 2006, 2007), and is also suggested by geophysical modelling (Hasenclever et al., 2014).

Bosch et al. (2004) and Nicolas et al. (2003) (and references therein) describe an interconnected seawater-derived hydrothermal system in the Samail Ophiolite (Sultanate of Oman), made up of gabbroic dykelets (recharge) and hydrothermal veins (discharge). Hydrothermal alteration occurs over a range of temperatures from very high temperatures (900–1020 °C) involving hydrous partial melting, down to lower temperature hydrothermal reactions at greenschist facies conditions (Bosch et al., 2004). In this study, we focus on the formation of amphiboles by hydrothermal fluid/rock interactions at different temperatures

* Corresponding author.
E-mail address: a.currin@mineralogie.uni-hannover.de (A. Currin).

https://doi.org/10.1016/j.lithos.2018.09.015
0024-4937/

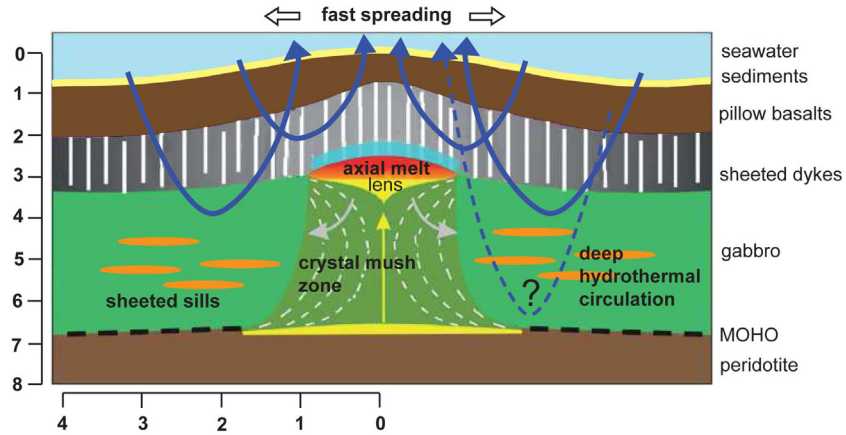

Fig. 1. Model showing the magma supply system at fast spreading MOR and hydrothermal circulation pathways (blue arrows), also involving the deep crust modified after Zhang et al. (2014).

between 500 and 1030 °C, through the detailed study of hydrothermal minerals formed in gabbros that crop out in the Wadi Wariyah, Wadi Tayin Massif, Samail Ophiolite (Sultanate of Oman).

Amphiboles are volatile-bearing minerals, and an important phase in the inventory of the partial hydration of the oceanic crust. They have been proven to be an important Cl reservoir in altered oceanic crust (e.g., Ito et al., 1983; Straub and Layne, 2003; Zhang et al., 2017a), since the structural site that can host $(OH)^-$ groups in amphibole can also accommodate Cl^- anions, as well as F− (Chan et al., 2016; Oberti et al., 1993; Vanko, 1986). Amphiboles are stable over a wide range of temperatures, and their compositional changes provide useful information on the temperature of fluid-rock interactions that resulted in their formation (e.g., Ernst and Liu, 1998). The occurrence of Cl-bearing amphibole in high temperature hydrothermal veins hosted in deep layered gabbros may suggest the presence of seawater-derived aqueous fluids and brines flowing down to the base of the oceanic crust (e.g., Manning et al., 1996; Coogan et al., 2001; Gillis and Meyer, 2001; Gillis et al. 2002; Bosch et al., 2004; Tribuzio et al. 2014). Consequently, by investigating such Cl-rich amphiboles and associated minerals, we can gain insight into the hydrothermal processes occurring in the lower oceanic crust.

The passage of fluids through different lithologies of the oceanic crust results in reactions with the host rock minerals. In addition, variations in composition, temperature, and pressure of the fluid lead to changes in fluid salinity, solute composition and fluid oxygen fugacity.

Our study focuses on high temperature hydrothermal veins and gabbroic dykelets hosted in the layered gabbro section of the Samail Ophiolite that contain different types of amphibole. We explore the influence of fluids on amphibole genesis at depth, and attempt to determine the origin of the fluids reacting with the lower oceanic crust using Sr and O isotopic analysis. Electron back-scatter diffraction (EBSD) analyses are integrated with chemical data to determine orientation differences between magmatic amphiboles and Cl-rich and Cl-poor hydrothermal amphiboles.

2. Analytical techniques

Polished thin sections of the rock samples were made of the hydrothermal veins and dykelets and areas around them. Mineral major element compositions were determined in situ using a Cameca SX100 electron microprobe equipped with 5 spectrometers and "Peak Sight" software at the Institute of Mineralogy of the Leibniz University Hannover, Germany. A focussed beam current of 15 nA and an acceleration voltage of 15 kV were used to analyze all minerals. Counting time for minerals was 10s for peak and 5 s for background, but was longer for Cl and F (30s peak). Elemental measurements were calibrated using the following natural and synthetic standards: albite (Na), wollastonite (Ca and Si), orthoclase (K), Durango apatite (P), Al_2O_3 (Al), Mn_2O_3 (Mn), TiO_2 (Ti), MgO (Mg), Fe_2O_3 (Fe), NaCl (Cl), and SrF_2 (F). In order to monitor analytical precision, each measurement was checked against the following international mineral standards (reference materials): Lake County plagioclase (USNM 115900), Kakanui hornblende (USNM 143965), Kakanui augite (USNM 122142), San Carlos Olivine (NMNH 111312-44), (Jarosewich et al., 1980). Detection limits (in wt%) in amphibole were: SiO_2: 0.03; TiO_2: 0.02; Al_2O_3: 0.03; FeO: 0.09, MnO: 0.05; MgO: 0.04; CaO: 0.04, NaO: 0.05; K: 0.015; Cr: 0.07; Cl: 0.007; F: 0.04. Representative values for measured amphiboles are listed in Table 1. The amphibole formula was calculated using 13 cations excluding Ca, Na and K., and the classification scheme used is that of Leake et al., 1997.

$^{87}Sr/^{86}Sr$ radiogenic isotope analyses of amphiboles, whole vein and whole dykelet samples were performed at the University of Southampton by thermal ionisation mass spectrometry (TIMS) using a ThermoFisher Scientific TritonPlus. Mineral separates were crushed and digested using a standard HF-HNO_3 acid attack, mother solutions were prepared (Zihlmann et al., 2018) and bulk trace element compositions were measured from diluted daughter solutions, using a ThermoScientific X-Series 2 ICP-MS adjusted for REE measurements prior to isotope analysis. Strontium spec™ columns were then used to separate Strontium from dissolved samples (Harris et al., 2015). The Sr concentrate was loaded onto degassed tantalum filaments for analysis by TIMS. Good internal precision was ensured by measuring 150 ratios per sample and presented given as two standard errors. The $^{87}Sr/^{86}Sr$ ratio of standard reference material NBS987 was measured as a monitor of external precision. Over the duration of the analyses it returned 0.710247 ± 0.000023 (2σ; $n = 53$).

The oxygen isotopic compositions of the same mineral separates as used for Sr-isotopes were determined by Actlabs (Activation Laboratories Ltd., Ancaster, Ontario, Canada). Oxygen was extracted from 5 mg samples at 550–600 °C according to the conventional BrF5 procedure of Clayton and Mayeda (1963) and analyzed via dual inlet on a Thermo-Finnigan DeltaPlus XP Isotope-Ratio Mass Spectrometer (IRMS). Results are calibrated to certified reference materials, relative to the VSMOW and VSLAP international standards. Precision and accuracy (standard deviation) are of 0.1‰.

Electron backscattered diffraction (EBSD) analyses were performed at the facilities of Montpellier University, France using a CamScan X500FE CrystalProbe with an Oxford/HKL EBSD system. This equipment allows for high resolution EBSD measurements (10–50 nm) and includes Energy Dispersive Spectrometry (EDS). The EBSD software used is AZtecHKL by Oxford Instruments for data acquisition and the Matlab-based code MTEX for analysis (see Ferrando et al., 2018).

Table 1
EPMA analyses of amphiboles from Wadi Wariyah (representative analyses).

			wt%													T position[e]		C position							B position			A position			W position		
Sample name	Temp. (°C) [a]	Amph. Name [b]	SiO_2	TiO_2	Al_2O_3	Cr_2O_3	MnO[c]	FeO[d]	MgO	CaO	Na_2O	K_2O	Cl	F	Total	Si	Al	Ti	Al	Cr	Fe^{3+}	Mn^{2+}	Fe^{2+}	Mg	Mg	Ca	Na	Na	K	Cl	OH	F	Mg#
WA02	545	Hs	39.74	0.3	9.35	0	0.15	23.17	7.09	11.67	1.9	1.05	4.33	0.22	98.97	6.37	1.63	0.04	0.14		0.60	0.02	2.51	1.70	0.00	2.00	0.00	0.59	0.22	1.18	0.71	0.11	40.3
WA02	660	Mhb	48.65	0.89	6.92	0.07	0.08	10.09	16.34	11.98	1.5	0.21	0.28	0.12	97.13	7.00	1.00	0.10	0.17	0.01	0.49	0.01	0.73	3.50	0.00	1.85	0.15	0.26	0.04	0.07	1.88	0.06	82.8
WA02	867	Ts	44.64	2.26	10.15	0	0.13	9.81	15.46	11.49	2.26	0.4	0.08	0.13	96.81	6.47	1.53	0.25	0.21		0.55	0.02	0.64	3.34	0.00	1.79	0.22	0.42	0.07	0.02	1.92	0.06	83.9
WA02	751	Mhb	44.79	1.43	9.48	0.06	0.08	13.89	13.22	11.77	2.05	0.25	1.19	0.16	98.37	6.58	1.42	0.16	0.22	0.01	0.53	0.01	1.17	2.90	0.00	1.85	0.15	0.44	0.05	0.30	1.63	0.07	71.2
WA02	1008	Mhs	42.74	3.96	12.17	0.06	0.13	10.67	14.27	11.64	2.62	0.24	0.06	0.08	98.64	6.15	1.86	0.43	0.21	0.01	0.43	0.02	0.86	3.06	0.00	1.79	0.21	0.52	0.05	0.01	1.95	0.04	78.1
WA05	716	Mhb	49.08	1.21	6.77	0.01	0.18	8.84	17.32	11.90	1.50	0.08	0.19	b.d. [f]	97.08	6.99	1.02	0.13	0.12	0.00	0.58	0.02	0.48	3.67	0.00	1.81	0.19	0.23	0.01	0.05	1.95		88.5
WA05	768	Mhs	43.45	1.54	10.95	0.03	0.05	10.21	14.78	11.98	2.43	0.14	0.79	b.d.	96.35	6.41	1.59	0.17	0.31	0.00	0.43	0.01	0.83	3.25	0.00	1.89	0.11	0.59	0.03	0.20	1.80		79.7
WA04	488	Prg	40.66	0.03	12.11	0.00	0.10	16.93	9.84	11.96	1.86	0.68	4.04	b.d.	98.21	6.30	1.70	0.00	0.51		0.51	0.01	1.68	2.27	0.00	1.99	0.01	0.54	0.14	1.06	0.94		57.5
WA04	630	Mhs	44.14	0.73	11.51	0.10	0.12	9.69	15.36	12.45	2.35	0.06	0.96	b.d.	97.46	6.42	1.58	0.08	0.39	0.01	0.47	0.01	0.71	3.33	0.00	1.94	0.06	0.60	0.01	0.24	1.76		82.5
WA04	1013	Prg	42.00	4.07	11.95	0.43	0.18	9.45	14.18	11.65	2.84	0.20	0.03	0.07	97.07	6.16	1.84	0.45	0.22	0.05	0.17	0.02	0.99	3.10	0.00	1.83	0.17	0.64	0.04	0.01	1.96	0.03	75.8
WA32	537	Fe-Prg	38.23	0.26	12.14	0.05	0.09	22.12	6.31	12.22	2.16	0.84	5.18	b.d.	99.61	6.15	1.85	0.03	0.46	0.01	0.26	0.01	2.72	1.51	0.00	2.00	0.00	0.68	0.17	1.41	0.59		35.7
WA32	523	Mhb	50.45	0.19	5.46	0.05	0.23	12.54	14.80	12.78	0.62	0.03	0.32	b.d.	97.48	7.30	0.70	0.02	0.23	0.01	0.27	0.03	1.24	3.19	0.00	1.98	0.02	0.16	0.01	0.08	1.92		72.0
WA32	547	Mhb	46.82	0.31	9.67	0.00	0.04	8.99	17.17	11.58	2.13	0.10	0.26	b.d.	97.08	6.64	1.36	0.03	0.26		0.90	0.01	0.17	3.63	0.00	1.76	0.24	0.35	0.02	0.06	1.94		95.6
WA33	1025	Mhs	41.16	4.45	12.40	0.05	0.15	9.82	14.32	11.45	3.16	0.11	0.01	b.d.	97.08	6.02	1.98	0.49	0.16	0.01	0.33	0.02	0.87	3.12	0.00	1.80	0.21	0.69	0.02	0.00	2.00		78.1
WA42	582	Prg	38.85	0.48	14.60	0.06	0.09	16.79	9.21	11.97	2.43	0.61	4.18	b.d.	99.27	5.99	2.01	0.06	0.64	0.01	0.45	0.01	1.72	2.12	0.00	1.98	0.02	0.70	0.12	1.09	0.91		55.2
WA42	642	Mhb	48.64	0.79	7.60	0.07	0.09	7.05	18.91	12.71	1.58	0.08	0.30	0.07	97.91	6.84	1.16	0.08	0.10	0.01	0.60	0.01	0.23	3.97	0.00	1.92	0.08	0.35	0.02	0.07	1.90	0.03	94.6
WA42	672	Ts	42.77	0.96	14.68	0.13	0.11	11.82	14.77	10.67	0.59	0.08	1.22	0.12	97.90	6.07	1.93	0.10	0.52	0.02	1.40		0.00	2.95	0.18	1.62	0.16	0.00	0.01	0.29	1.66	0.05	100.0
WA42	982	Mhs	42.42	3.48	11.61	0.10	0.13	10.19	15.42	12.01	3.00	0.13	0.02	0.05	98.57	6.10	1.90	0.38	0.07	0.01	0.51	0.02	0.71	3.31	0.00	1.85	0.15	0.69	0.02	0.01	1.97	0.02	82.3
WA46	558	Mhb	52.34	0.37	3.54	0.00	0.23	11.89	16.44	12.10	0.57	0.04	0.08	b.d.	97.59	7.44	0.56	0.04	0.04		0.60	0.03	0.82	3.49	0.00	1.84	0.16	0.00	0.01	0.02	1.98		81.0
WA46	900	Ts	44.63	2.55	9.20	0.06	0.18	11.82	14.62	11.24	1.91	0.69	0.15	b.d.	97.04	6.50	1.50	0.28	0.08	0.01	0.68	0.02	0.76	3.17	0.00	1.75	0.25	0.29	0.13	0.04	1.96		80.8

Values for the structual formula are atoms per formula unit (a.p.f.u.), calculated using a sum of 13 cations excluding Ca, Na, K.

[a] Temperatures calculated with Ti-in-hornblende thermometry (Ernst and Liu, 1998).

[b] According to mineral abbreviations by Whitney and Evans (2010). Prg: pargasite; Fprg: ferro-pargasite; Hst: hastingsite; Mhb: magnesio-hornblende; Mhs: magnesio-hastingsite; Ts: tschermakite.

[c] $MnO = MnO^{total}$

[d] $FeO = FeO^{total}$

[e] Amphibole positions in the structure.

[f] b.d.: below limit of detection.

3. Results

3.1. Outcrop description

The rocks cropping out in Wadi Wariyah (N 22°58′51.49“, E 58°15’53.98”), previously described by Bosch et al. (2004) and Wolff (2014), mainly consist of layered gabbro, crosscut by hydrothermal veins and cm-scale gabbroic dykelets, and are representative of deep oceanic crust, with rocks sampled ~ 100 m above the Moho transition zone (MTZ) (Fig. 2). Magmatic layering in the gabbros is approximately perpendicular to the strike of the overlying sheeted dykes in the area. The vein system displays a large variety of gabbroic dykelets and hydrothermal veins with different mineral fillings, including dykelets of several cm in width, mostly cutting the gabbro layering at high angles. These dykelets connect to each other in a system of branches (branched connectivity), and contacts, although sharp, do not show chilled margins. A second type of feature found in this outcrop are thin, black to dark green veins up to 4 mm wide that probably formed from the filling of microcracks, parallel to the gabbroic dykelets. These veins have sharp contacts to the host gabbro. The gabbroic dykelets and dark veins are clustered in several cm-wide swarms with single dykelets and veins spaced every few cm within the swarms, and swarms are spaced up to several metres apart. Both gabbroic dykelets and dark veins are roughly perpendicular to the gabbro layering and subparallel to each other. A third type of hydrothermal veins are white veins dominated by epidote/clinozoisite and/or prehnite that formed at lower temperatures. These white veins cross-cut the aforementioned dark veins and gabbroic dykelets. For details of this outcrop including images see Wolff (2014) and Bosch et al. (2004), and more details on the system of veins and dykelets see Nicolas et al. (2003). In this study we present data from dark veins (2 samples; Fig. 3A, C) and gabbroic dykelets (5 samples; Fig. 3B, D). Samples were collected within an area of 50 m (width) by 20 m (height) comprised of layered gabbro.

3.2. Petrography and amphibole composition (major and minor elements)

The host rock is a layered olivine gabbro containing olivine, clinopyroxene, and plagioclase, with small amounts of Fe-Ti oxides and orthopyroxene. The magmatic foliation of the gabbro is defined by orientated olivine and plagioclase crystals. The average grain size of the host rock minerals is ~1.5 mm. The dark veins and gabbroic dykelets contain different types of amphiboles (pargasite, magnesiohastingsite, magnesiohornblende, actinolite, hastingsite and ferropargasite), and some of them are highly enriched in chlorine (Table 1).

Specimens WA02 and WA05 were sampled from a high temperature hydrothermal vein containing mainly high-Ti pargasite (Ti >0.45 a.p.f.u.). Some pargasite grains are partially replaced (multiple zoning, Fig. 3A) and display the transition from high-Ti pargasite via replacive magnesiohastingsite and green magnesiohornblende to actinolite within a single grain, and locally, areas with greenish-blue Cl-rich ferropargasite and hastingsite with chlorine contents of up to 1.5 a.p.f.u. (atoms per formula unit), forming complex replacive textures (Figs. 4 & 5). In sample WA02, the grain size of the vein minerals is an average of 2 mm. The magmatic minerals that make up the host layered gabbro mainly have large grain sizes of about 2 to 3 mm. However, zoning within amphibole can be as small as ~5 μm.

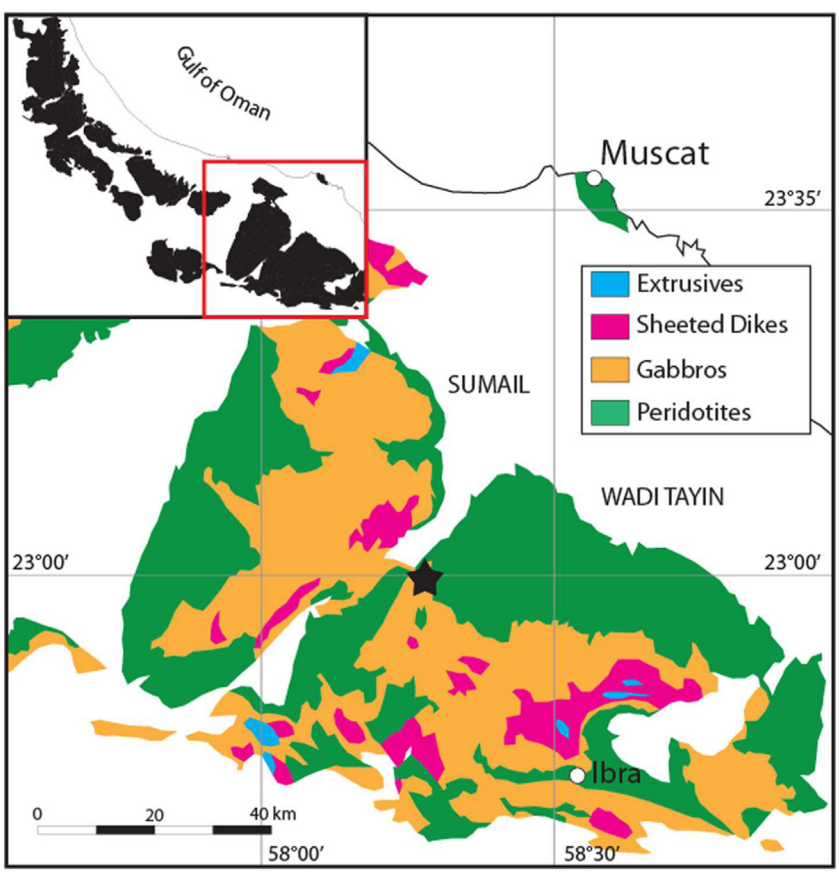

Fig. 2. Map of sampling location in Wadi Wariyah (star), in Wadi Tayin Massif, Samail Ophiolite, Sultanate of Oman, modified after Nicolas et al. (2000).

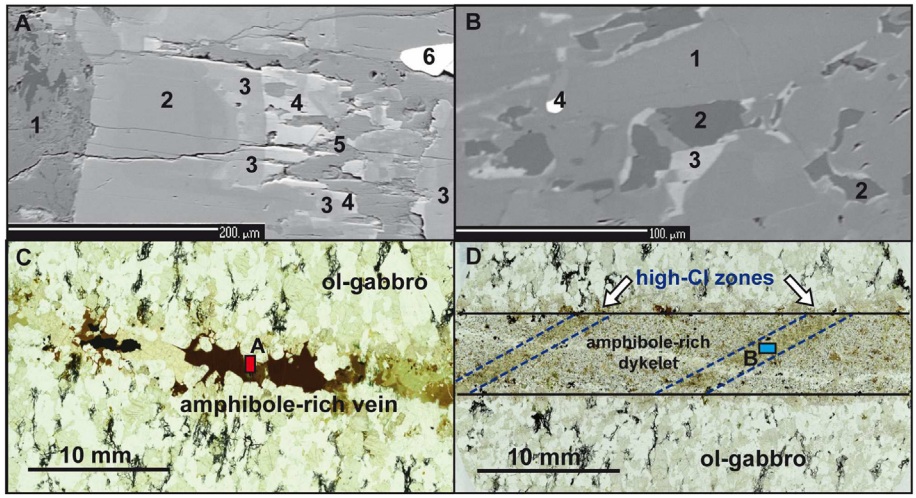

Fig. 3. A: BSE image showing the area marked in red in thin section C (sample WA02) showing a zoned amphibole. This is the same area selected for a compositional profile (Fig. 5). 1: plagioclase, 2: high-Ti pargasite, 3: magnesiohornblende to actinolite, 4: Cl-rich ferropargasite, 5: secondary calcite, 6: Fe—Ti oxides. **B**: BSE image showing the area marked in blue in thin section D (sample WA42). 1: pargasite, 2: plagioclase, 3: Cl-pargasite, 4: Fe—Ti oxides. **C**: thin section of layered olivine gabbro crosscut by an amphibole-rich hydrothermal vein (sample WA02). **D**: thin section of layered olivine gabbro crosscut by a fine-grained amphibole-rich gabbroic dykelet that is, in turn, crosscut by two oblique Cl-rich pargasite zones (sample WA42).

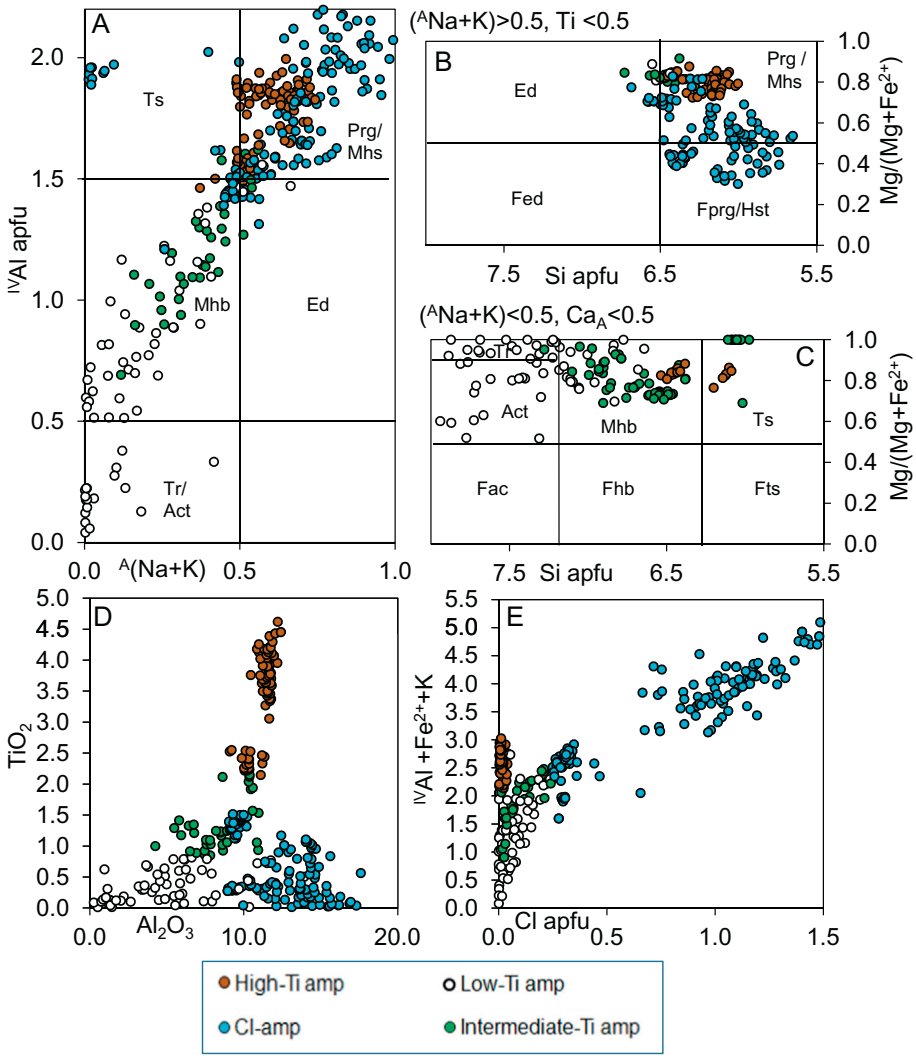

Fig. 4. Profile through an amphibole grain in sample WA02, ranging from magmatic high-Ti pargasite (D), through magnesiohornblende (C) and actinolite (B) to Cl-rich ferropargasite (A). Dashed and dotted black lines showing changes in amphibole zoning.

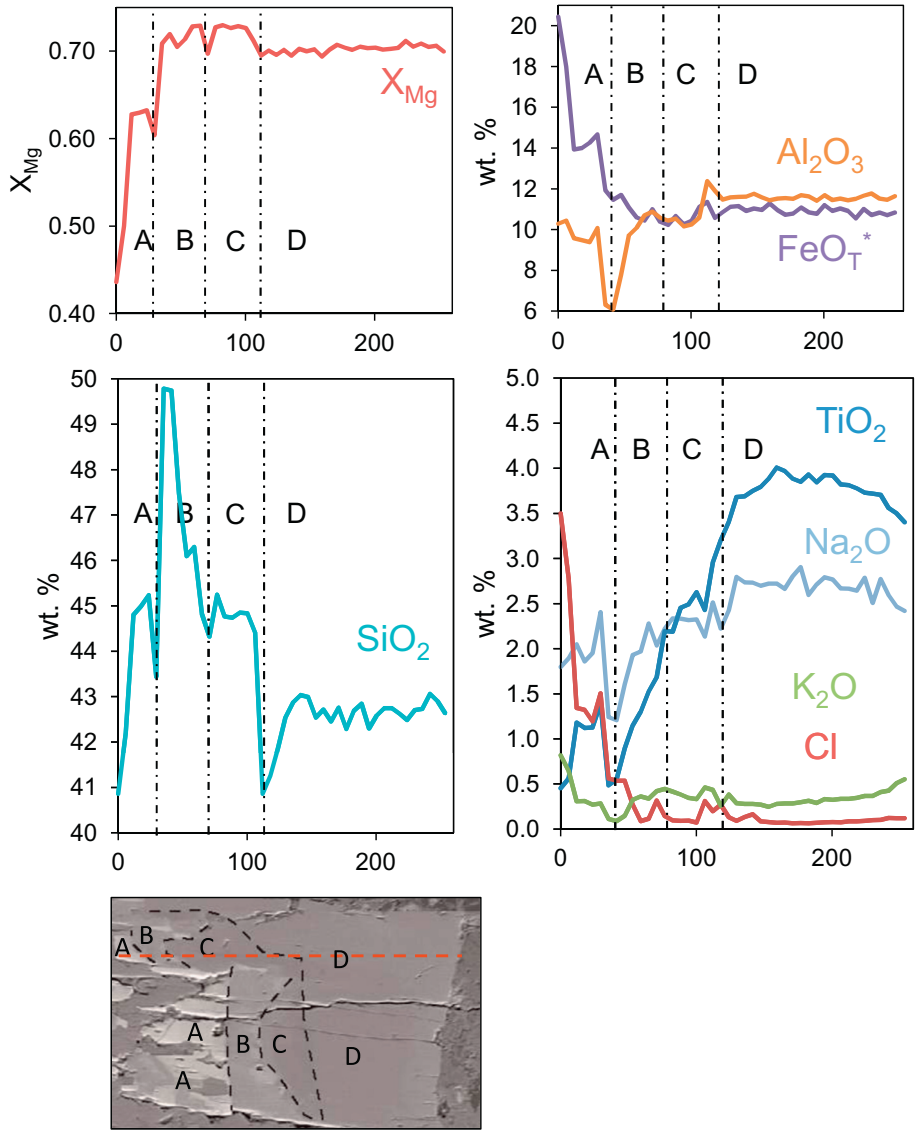

Fig. 5. Compositional diagrams for measured amphiboles. A: $^{A}(Na + K)$ vs. ^{IV}Al; B: Si a.p.f.u. vs. Mg# (Mg/(Mg + Fe^{2+})), with $^{A}(Na + K) > 0.5$, Ti < 0.5; C: Si a.p.f.u. vs. Mg# (Mg/(Mg + Fe^{2+})), with $^{A}(Na + K) < 0.5$, $Ca_A < 0.5$; D: Al_2O_3 vs. TiO_2; E: Cl a.p.f.u. vs. $^{IV}Al + Fe^{2+} + K$. Abbreviations after Whitney and Evans 2010: Ts, tschermakite; Mhs, magnesiohastingsite; Prg, pargasite; Mhb, magnesiohornblende; Tr, tremolite; Act, actinolite; Fed, ferro-edenite; Fprg, ferropargasite; Hst, hastingsite; Fac, ferro-actinolite; Fts, ferrotschermakite; Fhb, ferrohornblende.

Specimens WA42, WA04, WA33, WA46, and WA32A are samples of gabbroic dykelets. Thesesamples display poikilitic to fine-grained granular textures. Typically anhedral, mm-sized brown pargasitic amphibole forms poikilitic clusters, enclosing lath-shaped plagioclase chadacrysts and uncommon granular olivine, commonly associated with Fe-Ti oxides. Some plagioclase laths in the groundmass show swallowtail shapes indicating rapid cooling during formation. The amphiboles in these dykelets are of different types: Brown high-Ti pargasite and magnesiohastingsite (commonly poikilitic), green amphibole (mainly magnesiohornblende) replacing brown pargasite, and local occurrences of a distinctive bluish-green Cl-rich amphibole (WA04 & WA42: Cl-rich pargasite; WA32A: Cl-rich hastingsite). Microveins of green amphibole and amphibole overgrowths (hornblende and actinolite) in these dykelets are common. Sample WA42 displays chlorine-rich amphibole grains concentrated along two elongated and parallel amphibole-rich, high-Cl zones, formed oblique to the margins of the dykelet (Fig. 3). The high-Ti pargasites can have grain sizes of up to 150 μm whereas the other amphiboles have grain sizes between 10 and 50 μm. Serpentinite minerals occur locally as secondary phases reflecting a later stage of hydrothermal alteration, as seen from cross-cutting relationships between serpentine veins and amphiboles.

Amphiboles measured in both veins and dykelets display similar compositional characteristics, their main differences are textural, since gabbroic dykelets generally have finer grained amphibole. The analysis of different amphibole types including magmatic and hydrothermal amphibole reveals a large range of compositions (Table 1). High-Ti pargasite and magnesiohastingsite of magmatic origin have high ^{IV}Al contents (1.5 to 1.9 a.p.f.u). A-site occupancy (Na + K) in this group of amphiboles ranges from 0.37 to 0.74, with total Na of 0.5 to 0.9 a.p.f.u. and K < 0.1 a.p.f.u. Ti contents are between 0.24 a.p.f.u. and 0.5 a.p.f.u., and Cl contents range from 0.01 to 0.04 a.p.f.u., with no apparent correlation between Cl content and ^{IV}Al, Fe^{2+} and K (Fig. 4). Formation temperatures calculated for these amphiboles using Ti-in-amphibole thermometry (Ernst and Liu, 1998) range from 850 to 1030 °C. This thermometer is semi-quantitative, i.e. temperatures given here are only an approximation. The compositional heterogeneities between amphiboles indicate conditions of chemical disequilibrium, and thus the use of quantitative thermometers was not successful.

Pargasite, magnesiohastingsite, and edenite occurring in the gabbroic dykelets and veins are light brown to green. This group of amphiboles has ^{IV}Al contents ranging from 0.7 to 1.6 a.p.f.u. A-site occupancy (Na + K) ranges from 0.12 to 0.61, with total Na of 0.26 to 0.7 a.p.f.u.

and K < 0.1 a.p.f.u. These amphiboles have Ti contents between 0.07 and 0.28 a.p.f.u. Cl concentrations range from 0 to 0.25 a.p.f.u. There is an overall trend of increasing ^{IV}Al, Fe^{2+} and K with increasing Cl from a.p.f.u. 0.05 onwards. Below this Cl concentration there is no correlation between Cl content and ^{IV}Al, Fe^{2+} and K (Fig. 4). Temperatures calculated for these amphiboles range from 650 °C to 850 °C (Ti in amphibole thermometer) corresponding to the transition between magmatic and amphibolite facies metamorphic conditions.

Blue-green amphiboles have high concentrations of Cl (contents above 0.25 a.p.f.u.) and occur as rims around other amphibole grains or as fine-grained crystals. They are low in Si and high in ^{IV}Al compared to other amphiboles with lower Cl contents. Tetrahedral Al contents range from 1.2 to 2.3 a.p.f.u. They are mainly classified as Cl-bearing pargasite, Cl-bearing magnesiohastingsite, Cl-bearing hastingsite and Cl-bearing ferropargasite (Fig. 4). A-site occupancy (Na + K) in the measured amphiboles ranges from 0.17 to 1 a.p.f.u., with Na contents between 0.16 and 0.85 a.p.f.u., and K contents between 0.01 and 0.24 a.p.f.u. Ti contents are below 0.16 a.p.f.u. Cl contents in this group of amphiboles ranges from 0.25 up to 1.5 a.p.f.u. Cl. There is an overall trend of increasing ^{IV}Al, Fe^{2+} and K with increasing Cl. Formation temperatures for these amphiboles, calculated using Ti in amphibole thermometry, range from 484 to 765 °C (Ernst and Liu, 1998). The highest Cl contents (>1 a.p.f.u. Cl) are measured in amphibole grains formed at temperatures below 650 °C (see Table 1), at amphibolite to greenschist facies conditions.

Green actinolite, tremolite and magnesiohornblende form overgrowths over pargasite and magnesiohastingsite. These overgrowths are high in Si and low in ^{IV}Al compared to other amphiboles described in this section. Tetrahedral Al contents range from 0 to 1.6 a.p.f.u. Total Na ranges from 0 to 0. 7 a.p.f.u., with K < 0.04 a.p.f.u. Ti contents are found below 0.11 a.p.f.u. Maximum Cl content is of 0.25 a.p.f.u. There is an overall trend of increasing ^{IV}Al, Fe^{2+} and K with increasing Cl from a.p.f.u. 0.05 onwards. Below this value, there is no apparent trend (Fig. 4). Formation temperatures for these amphiboles are estimated between 484 °C and 646 °C from Ti in amphibole thermometry (Ernst and Liu, 1998), indicating hydrothermal alteration at amphibolite to greenschist facies conditions.

Fig. 5 shows a typical situation of an amphibole crystal displaying zoning, with different zones formed under different conditions, and a compositional profile through the zoned grain from a hydrothermal vein hosted in layered gabbro (sample WA02). This profile shows (A) a Cl-hastingsite zone (Cl contents up to 0.9 a.p.f.u.) with low silica content and high aluminum, as well as noticeably high total Fe and low Ti, corresponding to metamorphic conditions (amphibolite to greenschist facies); (B) a low-temperature actinolite zone (greenschist facies); (C) a magnesiohornblende zone with intermediate Cl contents (0.06 to 0.25 a.p.f.u.) with higher Si content and poor in Ti (amphibolites facies); and (D) a zone of brown high-Ti pargasite.

3.3. EBSD analyses

To determine whether Cl-rich and Cl-poor amphiboles have the same orientation, we obtained EBSD maps of areas containing amphiboles with different compositions, and compared the misorientations in a chosen area with the Cl-concentration map (EDS) of the same area (Fig. 6). Misorientations observed in zoned amphibole in relation to a point selected in a Cl-rich area (>0.7 a.p.f.u. Cl) are of 1 to 2° (Fig. 6, Mis2Mean map). Area 1 in Fig. 6D shows a misorientation boundary line with the same shape as the boundary between different domains of high and low Cl concentrations (Fig. 6C). This is also the case of the area circled in Figs. 6A and B, where changes in Cl content coincide with misorientations.

Point 2 in Fig. 6D shows a misorientation boundary line that coincides with a change in Cl content in Fig. 6C. In contrast, Point 3 in Fig. 6D shows only a gradual change in misorientation, but a more

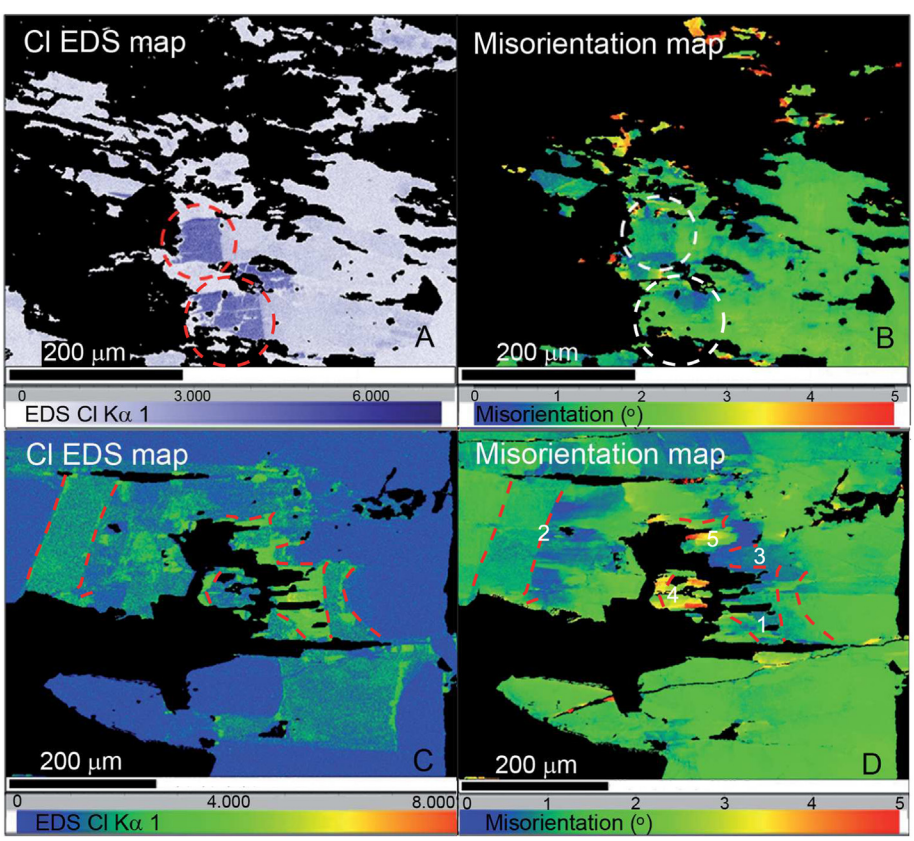

Fig. 6. Chlorine EDS maps (A & C) and EBSD misorientation maps of areas in sample WA02. Chlorine maps highlight the areas most enriched in Cl (A: purple, C: bright green). In contrast with EBSD misorientation maps (B & D) we can figure out if there are differences in orientation, grain boundaries or dislocations between Cl-rich areas and Cl-poor areas of the amphibole

pronounced change in Cl content in Fig. 6C. Points 4 and 5 highlight areas where there is no relationship between the misorientation map (Fig. 6D) and the distribution of Cl concentrations (Fig. 6C).

3.4. Isotopic data

3.4.1. Sr isotopes

$^{87}Sr/^{86}Sr$ radiogenic isotope analyses were carried out on amphiboles from both gabbroic dykelets and dark veins. We divided our samples into three groups: dark brown amphiboles (high-Ti pargasite and magnesiohastingsite) formed at magmatic temperatures >850 °C, green and blue-green amphiboles (magnesiohornblende and actinolite, and Cl-rich ferropargasite and hastingsite) formed at subsolidus temperatures between 550 and 750 °C, and whole rock samples (dark vein and gabbroic dykelet samples) (Fig. 7, Table 2).

Dark brown amphiboles contain 60 to 150 ppm Sr and show $^{87}Sr/^{86}Sr$ values between 0.7031 and 0.7035 (Table 2), similar to the green and blue-green amphiboles in the second group (Sr between 80 and 105 ppm; $^{87}Sr/^{86}Sr = 0.7032$ and 0.7036). Whole vein and dykelet analyses yield $^{87}Sr/^{86}Sr$ ratios between 0.7031 and 0.7039 (Sr concentration from 111 to 160 ppm).

The $^{87}Sr/^{86}Sr$ ratios of all the amphiboles measured are only slightly elevated compared to the range of fresh Oman rocks ($^{87}Sr/^{86}Sr$ ~0.7030; McCulloch et al., 1981) and there are no significant differences between the different amphibole groups. The slight increase in $^{87}Sr/^{86}Sr$ indicates only a minor exchange with seawater-derived Sr even for amphiboles with high Cl concentrations, suggesting fluid-rock exchange with seawater-derived hydrothermal fluids that had already reacted with a large amount of rock at low fluid/rock ratios (Fig. 7).

3.4.2. O isotopes

$\delta^{18}O$ values obtained for amphiboles fall in a narrow range between 4.1 and 5.6‰ except for one sample with a $\delta^{18}O$ of 7.3‰ (Fig. 7, Table 2). Values obtained from veins fall between 4.1 and 4.7, and values from gabbroic dykelets range from 4.9 to 7.3. Using the amphibole formation temperatures estimated from semi-quantitative Ti-in-amphibole thermometry as starting point, we calculated the oxygen isotopic composition of the hydrothermal fluid in equilibrium with these minerals using the amphibole-water fractionation equation of Zheng (1993) (See supplementary data Table 2). If the formation temperatures are reasonable and the amphiboles have retained their original oxygen isotopic compositions and not been subject to low temperature isotopic exchange, they are in equilibrium with hydrothermal fluids with high $\delta^{18}O$ between 6.9 and 7.5‰. Given the semi-quantitative nature of the thermometer used, and the heterogeneity of the amphiboles used for isotope measurements, these values are only an approximation. The values obtained (see supplementary data) are very different from Late Cretaceous seawater ($\delta^{18}O = -1$‰; Gregory and Taylor, 1981) or the composition of ancient black smoker fluids that are typically 1 to <4‰ higher than co-existing seawater (see Shanks et al., 1995). This suggests that oxygen isotopic exchange occurred in a very rock dominated system at low water/rock ratios. Alternatively, if the fluids are similar to Late Cretaceous seawater or a black smoker-like fluid derived from seawater, the analyzed amphibole $\delta^{18}O$ suggests formation temperatures between 90 and 130 °C (Appendix A1).

4. Discussion: Episodes of fluid/rock interaction

In addition to textural observations (poikilitic amphibole) and semi-quantitative geothermometry, magmatically formed amphiboles and hydrothermal amphiboles formed at subsolidus temperatures from hydrothermal fluids can be distinguished by their Ti, Na, K, Si contents and Mg number, with hydrothermal amphiboles exhibiting higher Si contents and Mg numbers, but lower Ti, Na and K contents (Gillis et al., 2003). The occurrence of different amphibole types from supra- and subsolidus reactions in an alteration parageneses in gabbros is also documented in other studies of oceanic (e.g. Coogan et al., 2001; Silantyev et al., 2008; Vanko, 1986) and continental rocks (Enami et al., 1999; Liu et al., 2009; McCormick and McDonald, 1999), and from experimental investigations (e.g., Currin et al. 2018 suprasolidus experiments: Khodorevskaya and Aranovich, 2016; Koepke et al., 2004, 2007). The passage of hydrothermal fluids through the crust in different episodes

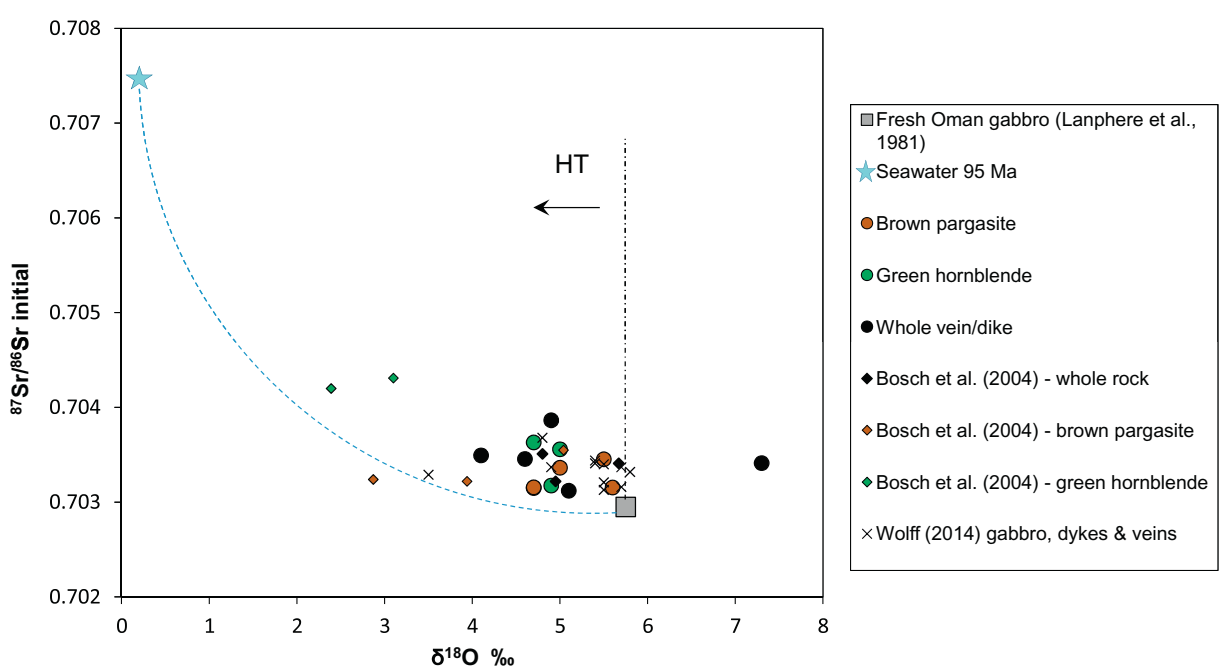

Fig. 7. Initial $^{87}Sr/^{86}Sr$ isotopic ratios plotted against $\delta^{18}O$ for amphibole and whole vein or dyke separates from high temperature veins and gabbroic dykelets of the Wadi Wariyah, Sultanate of Oman. Values for Cretaceous seawater at 95 Ma are from McArthur et al. (2001), and MORB mantle from Lanphere et al. (1981). Blue line: mixing curve of fresh Oman gabbro to seawater. Results are compared to measurements done by Wolff (2014) and Bosch et al. (2004).

Table 2
$^{87}Sr/^{86}Sr$, $\delta^{18}O$ (‰), Rb, Sr, and calculated W/R ratios for amphiboles, veins and dykelets from Wadi Wariyah.

Sample		Rb (ppm)	Sr (ppm)	$^{87}Rb/^{86}Sr$	$^{87}Sr/^{86}Sr$		$^{87}Sr/^{86}Sr_i$	$\delta^{18}O$ (‰)	W/R[b] 8 ppm[c]	W/R[b] 38 ppm[d]
WA02										
Prg[a], Mhs	A	0.784	64.26	0.0352	0.70317	± 1	0.70313	4.7	1.11	0.18
	B	0.771	64.76	0.0344	0.70318	± 1	0.70314		1.07	0.17
	C	0.764	73.09	0.0303	0.70323	± 1	0.70318		1.32	0.23
Mhb, Act, Cl-Hst		1.148	81.07	0.1505	0.70383	± 1	0.70363	4.7	4.95	0.76
Vein		0.525	138.2	0.0109	0.70347	± 1	0.70346	4.6	2.65	0.54
WA05										
Prg, Mhs		0.952	64.04	0.0429	0.70322	± 1	0.70316	4.7	1.27	0.21
Vein		0.376	159.5	0.0068	0.70350	± 1	0.70349	4.1	2.84	0.59
WA42										
Prg, Mhs		1.571	120	0.0377	0.70321	± 1	0.70316	5.6	1.22	0.20
Mhb, Act, Cl-Hst		1.396	101.3	0.0397	0.70323	± 1	0.70318	4.9	1.34	0.23
Dykelet		0.235	140.6	0.0048	0.70313	± 1	0.70312	5.1	0.83	0.17
WA04										
Prg, Mhs		0.786	116.5	0.0195	0.70348	± 1	0.70345	5.5	2.70	0.54
Mhb, Act, Cl-Hst		0.337	91.37	0.0106	0.70357	± 1	0.70356	5	3.25	0.67
Dykelet		0.417	111.5	0.0108	0.70388	± 1	0.70386	4.9	5.26	1.09
WA33										
Prg, Mhs		0.418	152	0.0079	0.70342	± 1	0.70341	5	2.18	0.43
Dykelet		0.728	122.8	0.0171	0.70339	± 1	0.70336	7.3	2.38	0.49

[a] According to the mineral abbreviations by Whitney and Evans (2010). Ed: Edenite; Fprg: ferro-pargasite; Hst: hastingsite; Mhb: magnesio-hornblende; Mhs: magnesio-hastingsite; Ts: tschermakite.

[b] Effective water/rock ratio mass balance calculation using the following equation (Taylor, 1977) $(W/R) = (^{87}Sr/^{86}Sr^{rock})_{final} - (^{87}Sr/^{86}Sr^{rock})_{initial} / (^{87}Sr/^{86}Sr^{seawater})_{initial} - (^{87}Sr/^{86}Sr^{rock})_{final}) \times (C^{rock}_{initial}(C^{seawater}_{initial})$.

[c] Using current (dynamic) 87Sr/86Sr, considering initial (95 Ma) of the rock (Lanphere et al., 1981) and initial seawater (McArthur et al., 2001), Sr concentration in the rock of 163 ppm (Kawahata et al. (2001) and current concentration in seawater of 8 ppm (Coogan et al., 2009).

[d] Using age-corrected 87Sr/86Sr for 95 Ma, considering initial (95 Ma) of the rock (Lanphere et al., 1981) and initial seawater (McArthur et al., 2001), Sr concentration in the rock of 163 ppm (Kawahata et al.,2001) and initial concentration in seawater of 38 ppm (Coogan et al., 2009).

with different temperatures and salinities is recorded by the formation of different amphibole types, equilibrating at progressively lower temperatures. This points towards the progressive cooling of the lower oceanic crust by involvement of hydrothermal fluids (Fig. 8).

Regarding microstructure, the subtle intragrain misorientations ilustrated in Fig. 6 are not large enough to account for different orientations at the time of mineral growth. Thus, Cl-rich ferropargasite and hastingsite may be epitactic with the other amphibole compositional zones. This may suggest that low-Ti amphiboles formed from the interaction of pre-existing magmatic amphibole with an aqueous Cl-rich fluid. Small orientation changes may be related to structural changes in the amphibole lattice due to Cl incorporation, or may be unrelated to mineral composition – possibly due to deformation of unknown origin. In some amphibole grains the misorientation boundary (see Fig. 6C) is not exactly coincident with the change in Cl content. This may be due to the fact that only higher Cl contents cause significant changes in the amphibole lattice (as present in the right hand side of Fig. 6) (see Oberti et al., 1993). Consequently, the misorientation of the amphibole structure due to Cl incorporation is only visible at higher Cl contents.

4.1. Suprasolidus

Considering the fine-grained granular texture of the aforementioned gabbroic dykelets, and considering previous experimental work done on the hydrous partial melting of gabbro (Koepke et al., 2004, 2005; Wolff, 2014), we consider that these dykelets were formed as products of hydrous partial melting of the host gabbro. The crystallization of brown high-Ti pargasite with poikilitic textures also implies that the magma they crystallized from was water-bearing (Fig. 8A), and their formation marks the onset of hydrothermal fluid-rock interactions at very high subsolidus to suprasolidus temperatures (850–1020 °C) in the described lithologies. $^{87}Sr/^{86}Sr$ values only slightly above 0.703 indicate Sr-isotopic exchange with a very rock-dominated fluid with only a hint of seawater-derived Sr.

4.2. Subsolidus

In contrast, the green amphibole zones appear to have formed from high temperature fluid-rock reactions occurring at upper amphibolite facies conditions (650–850 °C). In some samples, these dark veins retain relict amphibole cores that formed during the magmatic precursor stage.

Epitactic growth of Ti-poor and Cl-rich amphiboles (Fig. 8 B to D) suggests the occurrence of sub-solidus fluid-rock interactions at amphibolite facies.

The occurrence of Cl-rich amphibole domains (Fig. 8D) records the reaction between high Cl hydrothermal fluids or brines and pre-existing amphibole, albeit at low water/rock ratios. Finally, further fluid–rock exchange at lower amphibolite to greenschist facies temperatures is deduced from the presence of actinolite overgrowths (8E). This sequence of processes identified at the mm-scale illustrates the transition from the suprasolidus regime to the subsolidus regime in the presence of hydrothermal fluids percolating through the lower oceanic crust.

Correlations between Cl concentrations in amphibole and ^{IV}Al, Fe^{2+} and K contents are observed in Cl-rich amphiboles (up to 1.5 a.p.f.u. Cl, Fig. 4E), due to constraints in the amphibole structure and the larger size of the Cl^- anion with respect to OH^- (Oberti et al., 1993). For natural amphiboles from Wadi Wariyah, this correlation starts to be apparent for Cl contents >0.1 a.p.f.u. In amphiboles containing <0.1 a.p.f.u. Cl, the contents of ^{IV}Al, Fe^{2+} and K do not seem to be influenced by Cl incorporation. This also holds true for amphiboles obtained experimentally (Currin et al., 2018), which do not show any correlation between the aforementioned cations and Cl incorporation, since these amphiboles contain <0.1 a.p.f.u. Cl (Fig. 9). This lack of correlation between Cl and certain cations (e.g. Al, Fe, K) when small amounts of Cl are measured in the amphibole has also been reported in other natural Cl-bearing amphiboles (Enami et al., 1999; Kullerud, 1996), as well as in experimental studies (Chan et al., 2016).

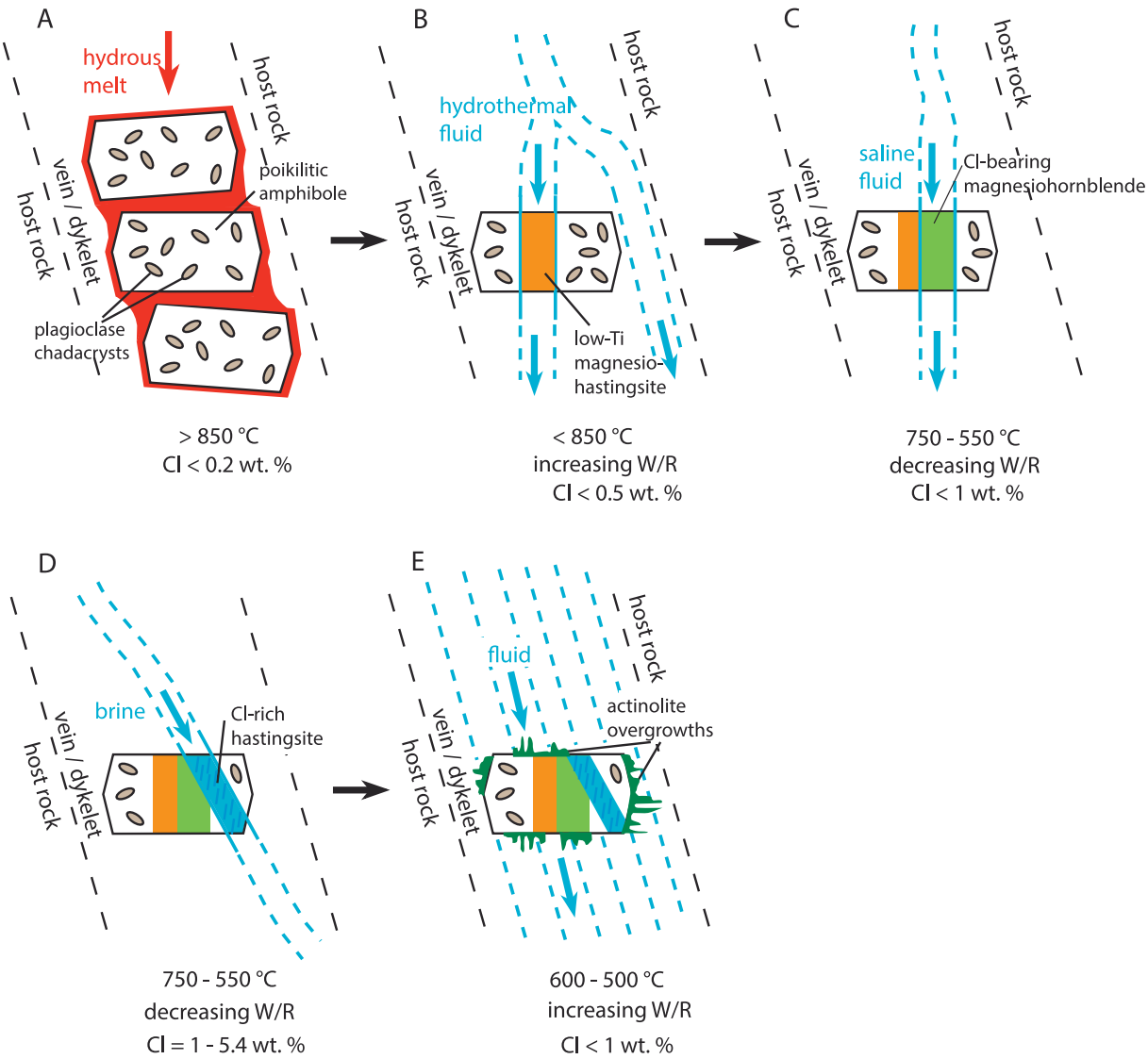

Fig. 8. Sketch showing the evolution of amphibole in gabbroic dykelets and dark veins in Wadi Wariyah. A: hydrous partial melting, formation of poikilitic magmatic amphibole – pargasite and magnesiohastingsite – in gabbroic dykelets and dark veins – amphibole is part of a dykelet that cross-cuts the host rock; red: represents the fine-grained matrix of the dykelets consisting of plagioclase, olivine, clinopyroxene, orthopyroxene, Fe-Ti oxides; Wolff, 2014. B: Dykelet flushing with the infiltration of a high-T hydrothermal fluid, heat removal, and metamorphism of vein and dykelet minerals. Formation of magnesiohastingsite containing Cl > 0.2 wt%. C: Dykelet flushing with the infiltration of a hydrothermal seawater-derived fluid, cooling and progressive concentration of Cl and decrease of water/rock ratio. Formation of magnesiohornblende containing Cl < 1 wt%. D: infiltration of highly concentrated saline fluid. Formation of hastingsite and ferropargasite containing Cl > 1 wt% up to 5.4 wt%. E: new episode of fluid infiltration at lower temperature – Cl-poor fluid – and formation of actinolite overgrowths.

The occurrence of Cl-rich amphiboles is linked to the participation of brines in fluid/rock interaction (Manning and Aranovich, 2014). This has also been shown in experiments performed with an NaCl, with the aim of producing Cl-rich amphibole, requiring supersaturated brines to succeed in producing amphiboles with Cl contents >0.1 a.p.f.u. Cl (Chan et al., 2016). This may suggest that amphiboles formed in nature also require reaction with a hydrothermal fluid that is saturated in Cl in order to reach high Cl contents, and this may be applied to the fluid that equilibrated with the rocks outcropping in Wadi Wariyah. Decrease of fluid/rock ratio is caused by the uptake of OH^- in the host rocks to form amphibole (amphibolitisation) and other hydrous minerals, as well as other processes elsewhere in the crust prior to reaching lower crustal gabbros (e.g. previous serpentinisation or greenstone alteration, Aranovich et al., 2010), with the subsequent concentration of Cl in the seawater-derived hydrothermal fluid, leading to the formation of brines that react with the host rock to form Cl-rich amphiboles.

Phase separation in saline fluids occurs below the critical curve that is found at different pressures for a given temperature – e.g. around 1.3 kbar for 750 °C and 20 wt% NaCl (Driesner and Heinrich, 2007). By crossing this curve towards lower pressures, a fluid will undergo phase separation into a NaCl-free vapour and a NaCl-concentrated fluid (i.e. brine). Pressures in the lower oceanic crust (ca. 6 km deep in the crust) are estimated at 2 kbar (Iturrino et al., 2002), and may vary due to exhumation and faulting of the oceanic crust, affecting fluid circulation and changing fluid behaviour, locally resulting in phase separation.

Large measured Cl quantities in amphibole from Wadi Wariyah (< 1.5 a.p.f.u.) confirms reaction with a seawater-derived fluid, and the isotopic signature of the amphibole (being relatively close to fresh Oman gabbro) suggests the environment was mostly rock-dominated and water/rock ratios were low during equilibration between fluid and amphibole. This is consistent with the findings of Bickle and Teagle (1992) for the Troodos ophiolite, and Gregory and Taylor (1981) for the Samail ophiolite, who also report on fluid-rock exchange at low water/rock ratios near the base of the crust, and Rospabé et al. (2017) who inferred the involvement of hydrothermal fluids in the mantle-crust transition in the Samail ophiolite.

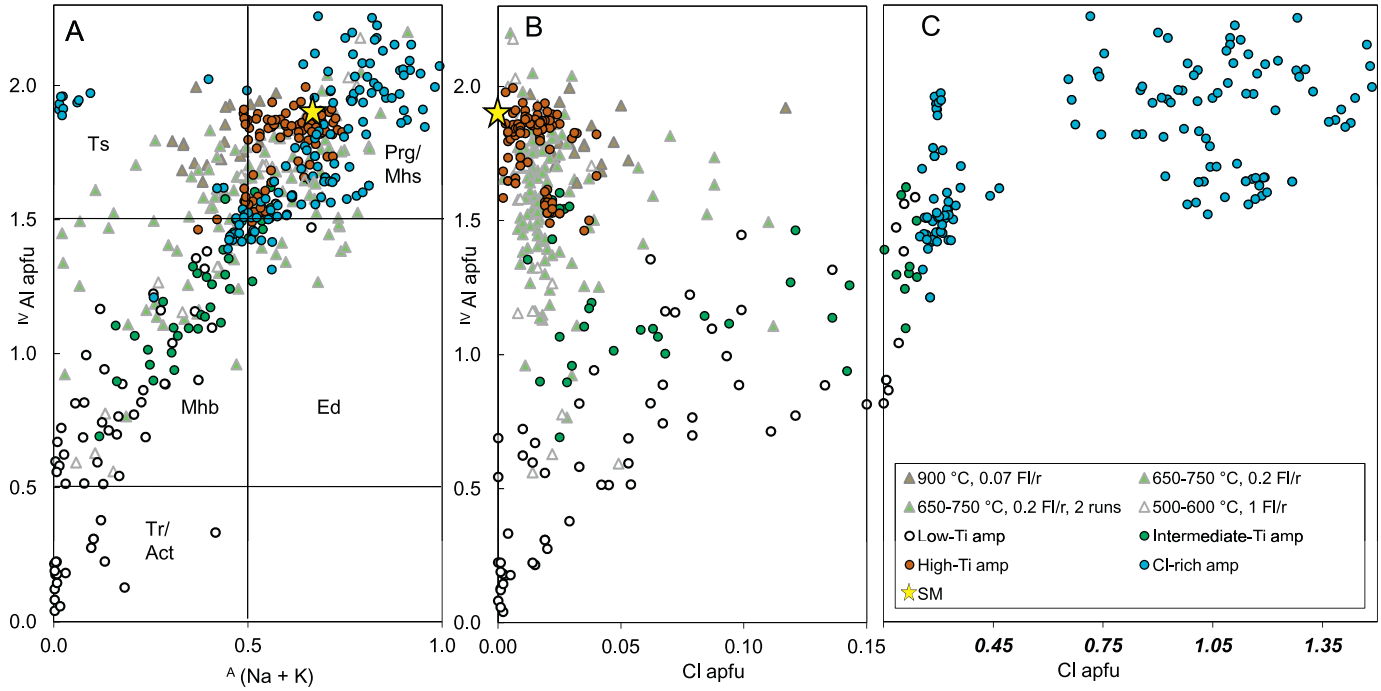

Fig. 9. Composition of amphiboles from Wadi Wariyah plotted against experimental results from Currin et al. (2018). Abbreviations after Whitney and Evans (2010): Ts, tschermakite; Mhs, magnesiohastingsite; Prg, pargasite; Mhb, magnesiohornblende; Tr, tremolite; Act, actinolite.

5. Concluding remarks

Amphiboles found in samples of hydrothermal veins and gabbroic dykelets from Wadi Wariyah, Samail Ophiolite, record a complex formation history involving fluid/rock interaction. These amphiboles are hosted within a hydrothermal microcrack system (Nicolas et al., 2003) and show a wide range of compositions from poikilitic high-Ti pargasite, via replacive magnesiohastingsite and magnesiohornblende, to Cl-rich hastingsite and Cl-poor actinolite, suggesting different episodes of hydrothermal activity at different temperatures. Variations in Cl content (from 0.02 to 1.5 a.p.f.u. Cl) and differences in Si, ^{IV}Al, Mg#, Na and K in amphibole, indicate equilibration of the host rock with fluids of different salinities at different points in time. In addition, EBSD analyses show compositional differences within single amphibole grains, confirming alteration of pre-existing magmatic amphibole by interaction with hydrothermal fluids. Near MORB-like $^{87}Sr/^{86}Sr$ ratios (0.7031 to 0.7039) and high $\delta^{18}O$ isotopic compositions (4.1–5.6) suggest the influence of a high-temperature seawater-derived fluid from magmatic (suprasolidus) to hydrothermal (subsolidus) temperatures, albeit in rock-dominated low fluid-rock ratio conditions, consistent with the presence of a highly saline fluid or brine. Our findings provide new petrological data on high temperature hydrothermal circulation present in the deep oceanic crust near fast-spreading ridges, and suggest an inhomogeneous distribution of hydrothermal fluid pathways in the lower oceanic crust, with stepwise fluid infiltration, and variations in fluid temperature and salinity.

Acknowledgements

The research leading to these results has received funding from the People Programme (Marie Curie Actions) of the European Union's Seventh Framework Programme FP7/2007-2013/ under REA grant agreement n608001, and from the Deutsche Forschungsgemeinschaft (DFG, KO1723/10-1). Many thanks to Julian Feige (Leibniz Universität Hannover) for thin section preparation, to Fabrice Barou (Géosciences Montpellier, CNRS) for help and technical support during EBSD analyses, to James Andy Milton (National Oceanography Centre Southampton) for assistance with the LA-ICP-MS, Matt Cooper (National Oceanography Centre Southampton) for assistance in the clean lab and operating the TIMS, and Aurélien Beaumais (National Oceanography Centre Southampton) for support in the clean lab. We also wish to thank Riccardo Tribuzio and the anonymous reviewer for their helpful comments and suggestions.

Appendix A. Supplementary data

Supplementary data to this article can be found online at https://doi.org/10.1016/j.lithos.2018.09.015.

References

Abily, B., Ceuleneer, G., Launeau, P., 2011. Synmagmatic normal faulting in the lower oceanic crust: evidence from the Oman ophiolite. Geology 39, 391–394.

Alt, J.C., Bach, W., 2006. Oxygen isotope composition of a section of lower oceanic crust, ODP Hole 735B. Geochemistry, Geophysics, Geosystems 7 (12), Q12008. https://doi.org/10.1029/2006GC001385.

Aranovich, L.Y., Bortnikov, N.S., Serebryakov, N.S., Sharkov, E.V., 2010. Conditions of the formation of plagiogranite from the Markov Trough, Mid-Atlantic Ridge, 5°52′–6°02′N. Doklady Earth Sciences 434 (Part 1), 1257–1262.

Bickle, M.J., Teagle, D.A.H., 1992. Strontium alteration in the Troodos ophiolite: implications for fluid fluxes and geochemical transport in mid-ocean ridge hydrothermal systems. Earth and Planetary Science Letters 113 (1–2), 219–237. https://doi.org/10.1016/0012-821X(92)90221-G ISSN 0012-821X.

Bosch, D., Jamais, M., Boudier, F., Nicolas, A., 2004. Deep and High-temperature Hydrothermal Circulation in the Oman Ophiolite - Petrological and Isotopic evidence. Journal of Petrology 45 (6), 1181–1208.

Chan, A., Jenkins, D.M., Dyar, M.D., 2016. Partitioning of Chlorine between NaCl Brines and Ferro-Pargasite: Implications for the Formation of Chlorine-Rich Amphiboles in Mafic Rocks. The Canadian Mineralogist 54 (1), 337–351.

Clayton, R.N., Mayeda, T.K., 1963. The use of Bromine Pentafluoride in the Extraction of Oxygen from Oxides and Silicates for Isotopic Analysis. Geochimica et Cosmochimica Acta 27, 43–52.

Coogan, L.A., Wilson, R.N., Gillis, K.M., MacLeod, C.J., 2001. Near-solidus evolution of oceanic gabbros: Insights from amphibole geochemistry. Geochimica et Cosmochimica Acta 65 (23), 4339–4357.

Coogan, L.A., Howard, K.A., Gillis, K.M., Bickle, M.J., Chapman, H., Boyce, A.J., Jenkin, G.R.T., Wilson, R.N., 2006. Chemical and thermal constraints on focussed fluid flow in the lower oceanic crust. American Journal of Science 306, 389–427.

Coogan, L.A., Manning, C.E., Wilson, R.N., 2007. Oxygen isotope evidence for short-lived high-temperature fluid flow in the lower oceanic crust at fast-spreading ridges. Earth and Planetary Science Letters 260, 524–536.

Coogan, L.A., 2009. Altered oceanic crust as an inorganic record of paleoseawater Sr concentration. Geochemistry, Geophysics, Geosystems 10, Q04001. https://doi.org/10.1029/2008GC002341.

Currin, A., Koepke, J., Almeev, R.R., Beermann, O., 2018. Interaction of highly saline fluid and olivine gabbro: Experimental simulation of deep hydrothermal processes involving amphibole at the base of the oceanic crust. Lithos https://doi.org/10.1016/j.lithos.2018.09.017 0024-4937.

Driesner, T., Heinrich, C., 2007. The system H2O–NaCl. Part I: Correlation formulae for phase relations in temperature–pressure–composition space from 0 to 1000°C, 0 to 5000bar, and 0 to 1 XNaCl. Geochimica et Cosmochimicha Acta 71 (20), 4880–4901.

Enami, M., Liou, J.G., Bird, D.K., 1999. Cl-bearing amphibole in the Salton Sea Geothermal System, California. Canadian Mineralogist 30, 1077–1092.

Ernst, W.G., Liu, J., 1998. Experimental phase-equilibrium study of Al- and Ti- contents of calcic amphibole in MORB. A semiquantitative thermobarometer. American Mineralogist 83, 952–969.

Ferrando, C., Godard, M., Ildefonse, B., Rampone, E., 2018. Melt transport and mantle assimilation at Atlantis Massif (IODP Site U1309) : Constraints from geochemical modeling. Lithos https://doi.org/10.1016/j.lithos.2018.01.012.

Gillis, K.M., Coogan, L.A., Chaussidon, M., 2003. Volatile element (B, Cl, F) behaviour in the roof of an axial magma chamber from the East Pacific rise. Earth and Planetary Science Letters 213, 447–462.

Gillis, K.M., Meyer, P.S., 2001. Metasomatism of oceanic gabbros by late stage melts and hydrothermal fluids: Evidence from the rare earth element composition of amphiboles. Geochemistry, Geophysics, Geosystems 2 2000GC000087.

Gregory, R.T., Taylor, H.P., 1981. An oxygen isotope profile in a section of cretaceous oceanic crust, Samail ophiolite, Oman: evidence for d18O buffering of the oceans by deep (45 km) seawater-hydrothermal circulation at mid-ocean ridges. Journal of Geophysical Research 86 (B4), 2737–2755.

Harris, M., Coggon, R.M., Smith-Duque, C.E., Cooper, M.J., Milton, J.A., Teagle, D.A.H., 2015. Channelling of hydrothermal fluids during the accretion and evolution of the upper oceanic crust: Sr isotope evidence from ODP Hole 1256D. Earth and Planetary Science Letters 416, 56–66.

Harris, M., Coggon, R.M., Wood, M., Smith-Duque, C.E., Henstock, T.J., Teagle, D.A.H., 2017. Hydrothermal cooling of the ocean crust: Insights from ODP Hole 1256D. Earth and Planetary Science Letters 462, 110–121.

Hasenclever, J., Theissen-Krah, S., Rüpke1, L.H., Morgan, J.P., Iyer, K., Petersen, S., Devey, C.W., 2014. Hybrid shallow on-axis and deep off-axis hydrothermal circulation at fast-spreading ridges. Letters to Nature 508, 508–512. https://doi.org/10.1038/nature13174.

Ito, E., Harris, D.M., Anderson, A.T., 1983. Alteration of oceanic crust and geologic cycling of chlorine and water. Geochimica et Cosmochimica Acta 47, 1613–1624.

Iturrino, G.J., Ildefonse, B., Boitnott, G., 2002. Velocity structure of the lower oceanic crust: results from Hole 735B, Atlantis II Fracture Zone. In: Natland, J.H., Dick, H.J.B., Miller, D.J., Von Herzen, R.P. (Eds.), Proceedings of the Ocean Drilling Program. vol. 176. Scientific Results, pp. 1–71.

Jarosewich, E., Nelen, J., Norberg, J.A., 1980. Reference samples for electron microprobe analysis. Geostandards Newsletter 4 (1), 43–47.

Kawahata, H., Nohara, M., Ishizuka, H., Hasebe, S., Chiba, H., 2001. Sr isotope geochemistry and hydrothermal alteration of the Oman ophiolite. Journal of Geophysical Research 106 (B6), 11083–11099. https://doi.org/10.1029/2000JB900456.

Khodorevskaya, L.I., Aranovich, L.Y., 2016. Experimental study of amphibole interaction with H2O–NaCl Fluid at 900°C, 500 MPa: toward granulite facies melting and mass transfer. Journal of Petrology 24 (3), 215–233.

Koepke, J., Feig, S.T., Snow, J., Freise, M., 2004. Petrogenesis of oceanic plagiogranites by partial melting of gabbros: an experimental study. Contributions to Mineralogy and Petrology 146, 414–432.

Koepke, J., Feig, S.T., Snow, J., 2005. Hydrous partial melting within the lower oceanic crust. Terra Nova 17, 286–291.

Koepke, J., Berndt, J., Feig, S.T., Holtz, F., 2007. The formation of SiO2-rich melts within the deep oceanic crust by hydrous partial melting of gabbros. Contributions to Mineralogy and Petrology 153, 67–84.

Kullerud, K., 1996. Chlorine-rich amphiboles; interplay between amphibole composition and an evolving fluid. European Journal of Mineralogy 8 (2), 355.

Lanphere, M., Coleman, R., Hopson, C., 1981. Sr isotopic tracer study of the Samail ophiolite, Oman. Journal of Geophysical Research 86 (B4), 2709–2720.

Leake, B.E., Woolley, A.R., Arps, C.E.S., Birch, W.D., Gilbert, M.C., Grice, J.D., Hawthorne, F.C., Kato, A., Kisch, H.J., Krivovichev, V.G., Linthout, K., Laird, J., Mandarino, J., Maresch, W.V., Nickel, E.H., Rock, N.M.S., Schumacher, J.C., Smith, D.C., Stephenson, N.C.N., Ungaretti, L., Whittaker, E.J.W., Youzhi, G., 1997. Nomenclature of amphiboles: Report of the subcommittee on amphiboles of the International Mineralogical Association Commission on New Minerals and Mineral Names. The Canadian Mineralogist 35, 219–246.

Liu, J., Liu, W., Ye, K., Mao, Q., 2009. Chlorine-rich amphibole in Yangkou eclogite, Sulu ultrahigh-pressure metamorphic terrane, China. European Journal of Mineralogy 21, 1265–1285.

Manning, C.E., Aranovich, L.Y., 2014. Brines at high pressure and temperature: Thermodynamic, petrologic and geochemical effects. Precambrian Research 253, 6–16.

Manning, C., MacLeod, C., 1996. Fracture-controlled metamorphism of Hess Deep gabbros, Site 894: constraints on the roots of mid-ocean-ridge hydrothermal systems at fast-spreading centers. In: Mével, C., Gillis, K.M., Allan, J.F., Meyer, P.S. (Eds.), Proceedings ODP, Scientific Results. Ocean Drilling Program, College Station, TX, pp. 189–212.

Manning, C., Weston, P., Mahon, K., 1996. Rapid high temperature metamorphism of East Pacific rise gabbros from Hess deep. Earth and Planetary Science Letters 144, 123–132.

Manning, C.E., MacLeod, C.J., Weston, P.E., 2000. Lower-crustal cracking front at fast-spreading ridges: Evidence from the East Pacific Rise and the Oman Ophiolite. In: Dilek, Y., Moores, E.M., Elthon, D., Nicolas, A. (Eds.), Ophiolites and oceanic crust: new insights from field studies and the Ocean Drilling Program. Special Paper of the Geological Society of America 349, pp. 261–272. https://doi.org/10.1130/0-8137-2349-3.261.

McArthur, J.M., Howarth, R.J., Bailey, T.R., 2001. Strontium isotope stratigraphy: LOWESS version 3: best fit to the marine Sr-isotope curve for 0–509 Ma and accompanying look-up table for deriving numerical age. The Journal of Geology 109, 155–170.

McCormick, K.A., McDonald, A.M., 1999. Chlorine-bearing amphiboles from the Fraser mine, Sudbury, Ontario, Cacnada: description and crystal chemistry. The Canadian Mineralogist 37, 1385–1403.

McCulloch, M., Gregory, R., Wasserburg, G., Taylor, H., 1981. Sm-Nd, Rb-Sr, and 18O/16O isotopic systematics in an oceanic crustal section- evidence from the Samail ophiolite. Journal of Geophysical Research 86, 2721–2735.

Nicolas, A., Boudier, F., Ildefonse, B., Bali, E., 2000. Accretion of Oman and United Arab Emirates ophiolite –Discussion of a new structural map. Marine Geophysical Research 21, 147–179.

Nicolas, A., Mainprice, D., Boudier, F., 2003. High temperature seawater circulation throughout crust of oceanic ridges. A model derived from the Oman ophiolite. Journal of Geophysical Research 108, 2371.

Oberti, R., Ungaretti, L., Cannillo, E., Hawthorne, F., 1993. The mechanism of Cl incorporation in amphibole. American Mineralogist 78, 746–752.

Rospabé, M., Ceuleneer, G., Benoit, M., Abily, B., Pinet, P., 2017. Origin of the dunitic mantle-crust transition zone in the Oman ophiolite: The interplay between percolating magmas and high-temperature hydrous fluids. Geology 45 (5), 471–474. https://doi.org/10.1130/G38778.1.

Shanks, W.C., Bohlke, J.K., Seal, R.R., 1995. Stable Isotopes in Mid-Ocean Ridge Hydrothermal Systems: Interactions between Fluids, Minerals, and Organisms. American Geophysical Union Geophysical, Washington DC, pp. 194–221.

Silantyev, S.A., Kostitsyn, Yu.A., Cherkashin, D.V., Dick, H.J.B., Kelemen, P.B., Kononkova, N.N., Kornienko, E.M., 2008. Magmatic and metamorphic evolution of the oceanic crust in the Western Flank of the MAR Crest Zone at 15° 44' N: Investigation of cores from sites 1275B and 1275D, JOIDES Resolution Leg 209. Petrology 16 (4), 353–375.

Straub, S.M., Layne, G.D., 2003. The systematics of chlorine, fluorine, and water in Izu arc front volcanic rocks: Implications for volatile recycling in subduction zones. Geochimica et Cosmochimica Acta 67, 4179–4203.

Taylor, H.P., 1977. Water/rock interactions and the origin of H2O in granitic batholiths. Journal of the Geological Society of London 133 (6), 509–558.

Tribuzio, R., Renna, M.R., Dallai, L., Zanetti, A., 2014. The magmatic–hydrothermal transition in the lower oceanic crust: Clues from the Ligurian ophiolites. Italy, Geochimica et Cosmochimica Acta 130, 188–211. https://doi.org/10.1016/j.gca.2014.01.010.

Vanko, D., 1986. High-chlorine amphiboles from oceanic rocks: product of highly saline hydrothermal fluids. American Mineralogist 71, 51–59.

Whitney, D.L., Evans, B.W., 2010. Abbreviations for names of rock-forming minerals. American Mineralogist 95, 185–187.

Wolff, P.E., 2014. Hydrothermal circulation from very high to low temperatures in the lower oceanic crust - Evidence from layered gabbros from the Oman Ophiolite and from partial melting experiments on oceanic gabbros. PhD Thesis. Leibniz Universität Hannover, p. 167.

Zhang, C., Koepke, J., Kirchner, C., Götze, N., Behrens, H., 2014. Rapid hydrothermal cooling above the axial melt lens at fast-spreading mid-ocean ridge. Scientific Reports 4, 6342. https://doi.org/10.1038/srep06342.

Zhang, C., Koepke, J., Albrecht, M., Horn, I., Holtz, F., 2017a. Apatite in the dike-gabbro transition zone of mid-ocean ridge: evidence for brine assimilation by axial melt lens. In: Harlov, D, and Hughes, J. (Eds.). Apatite: a common mineral, uncommonly versatile. American Mineralogist 102, 558–570.

Zhang, C., Wang, L.-X., Marks, M.A.W., France, L., Koepke, J., 2017b. Volatiles (CO2, S, F, Cl, Br) in the dike-gabbro transition zone at IODP Hole 1256D: Magmatic imprint versus hydrothermal influence at fast-spreading mid-ocean ridge. Chemical Geology 459, 43–60.

Zheng, Y.-F., 1993. Calculation of oxygen isotope fractionation in hydroxyl-bearing silicates. Earth and Planetary Science Letters 120, 247–263.

Zihlmann, B., Müller, S., Coggon, R.M., Koepke, J., Garbe-Schönberg, D., Teagle, D.A.H., 2018. Hydrothermal fault zones in the lower oceanic crust: An example from Wadi Gideah, Samail ophiolite. Lithos, Oman https://doi.org/10.1016/j.lithos.2018.09.008.